Original article

Discovery of N6-phenyl-1*H*-pyrazolo[3,4-d]pyrimidine-3,6-diamine derivatives as novel CK1 inhibitors using common-feature pharmacophore model based virtual screening and hit-to-lead optimization

Ling-Ling Yang [a,b,1], Guo-Bo Li [a,1], Heng-Xiu Yan [a,1], Qi-Zheng Sun [a], Shuang Ma [a], Pan Ji [a], Ze-Rong Wang [a], Shan Feng [a], Jun Zou [a], Sheng-Yong Yang [a,*]

[a] *State Key Laboratory of Biotherapy and Cancer Center, West China Hospital, West China Medical School, Sichuan University, #1 Keyuan Road 4, Sichuan 610041, China*
[b] *College of Chemical Engineering, Sichuan University, Sichuan 610041, China*

ABSTRACT

Aberrant activation of casein kinase 1 (CK1) has been demonstrated to be implicated in the pathogenesis of cancer and various central nervous system disorders. Discovery of CK1 inhibitors has thus attracted much attention in recent years. In this account, we describe the discovery of N6-phenyl-1*H*-pyrazolo[3,4-d]pyrimidine-3,6-diamine derivatives as novel CK1 inhibitors. An optimal common-feature pharmacophore hypothesis, termed Hypo2, was firstly generated, followed by virtual screening using Hypo2 against several chemical databases. One of the best hit compounds, N6-(4-chlorophenyl)-1*H*-pyrazolo[3,4-d]pyrimidine-3,6-diamine, was chosen for the subsequent hit-to-lead optimization under the guide of Hypo2, which led to the discovery of a new lead compound (1-(3-(3-amino-1*H*-pyrazolo[3,4-d]pyrimidin-6-ylamino)phenyl)-3-(3-chloro-4-fluorophenyl)urea) that potently inhibits CK1 with an IC$_{50}$ value of 78 nM.

1. Introduction

Protein kinase casein kinase 1 (CK1) belongs to the serine/threonine kinase superfamily that functions as a regulator of signal transduction pathways in most eukaryotic cell types [1]. CK1 isoforms, which are highly conserved in their kinase domains (53%–98% identical) but significantly differ in their regulatory C-terminal region, are involved in Wnt signaling, circadian rhythms, nucleo-cytoplasmic shuttling of transcription factors, DNA repair, and DNA transcription [1–3]. Aberrant functional regulation of CK1, such as its over-expression or excessive activation, has been demonstrated to be implicated in the pathogenesis of many diseases including Alzheimer's disease [4], Parkinson's disease [5], sleep disorders [6], inflammation [7] and cancers [8]. Thus CK1

inhibitors have been thought as promising interfering agents in the treatment and prevention of these diseases.

Due to the potential application of CK1 inhibitors in various diseases, the development of CK1 inhibitors have attracted much attention in recent years. Though some CK1 inhibitors have been reported, there is no CK1 inhibitor in clinical studies so far. Thus, discovering more potent CK1 inhibitors is still needed, which could provide more lead candidates for drug development. Formerly, the discovery of CK1 inhibitors was achieved through high-throughput screening (HTS) [9] and subsequent experience-based structural optimization, which usually suffered a high cost and a low success rate. Currently, the fast developing computer-aided drug discovery methods, including virtual screening [10–13] and quantitative structure–activity relationship (QSAR)-guided structural optimization [14–16], provide economic and rapid approaches to the lead discovery. In this investigation, we shall describe the discovery of N6-phenyl-1*H*-pyrazolo[3,4-d]pyrimidine-3,6-diamine derivatives as novel CK1 inhibitors, which were obtained through virtual screening based on a common-feature pharmacophore model of CK1 inhibitors, and subsequent pharmacophore model guided hit-to-lead optimization.

2. Results and discussion

2.1. Generation of common-feature pharmacophore model of CK1 inhibitors

In this section, we shall describe the development of a common-feature pharmacophore model of CK1 inhibitors. As one of the major computer-aided drug discovery methods, the pharmacophore method has been widely used in the virtual screening for retrieving hit compounds. A pharmacophore model could be developed by methods either ligand-based or complex-based [17]. Pharmacophore models developed by ligand-based methods could involve information from a broad range of active compounds contained in a so-called training set [18–20]. Nevertheless, the generated pharmacophore models might not correctly reflect the interaction mode between the ligands and target, which stems from the possible defects of algorithms for the ligand conformational generation. On the contrary, pharmacophore hypotheses built by complex-based methods are often directly derived from the interaction mode between the ligand and target in one complex, which inevitably leads to that the generated pharmacophore model contains very limited ligand information [17,21]. Apparently an ideal pharmacophore model should not only properly reflect the interaction mode between the ligand and receptor, but also contain information from more active compounds. Thus, in order to develop such an ideal pharmacophore model, we proposed a new pharmacophore modeling protocol for CK1 inhibitors, which is described as follows.

Firstly, all the publicly reported CK1 inhibitors were collected from literature [22–28]. Eight representative CK1 inhibitors were chosen to form a training set (see Chart 1); these compounds were selected since they are the most active compounds and each one of them possesses a different scaffold. Secondly, each compound in the training set was docked to the active site of CK1 (PDB: 2CSN) to form a ligand–receptor complex (see Fig. 1). Here the GOLD program was used since it is one of the best programs for flexible docking calculations [29]. Thirdly, each complex was taken as the input to create pharmacophore hypotheses by using the 'Receptor-Ligand Pharmacophore Generation' module in Discovery Studio

(DS) 3.1 program package. After the running of program, 10 pharmacophore hypotheses were created for each complex with the top ranking one being assigned as the final pharmacophore hypothesis for the corresponding complex, which are shown in Fig. 1. Fourthly, all of the eight pharmacophore hypotheses were superimposed together. Chemical features with the same property and same location in the three dimensional (3D) space were identified as common features, which were used for constructing the overall pharmacophore model with the aid of Hypoedit module within Catalyst (AccelrysR) (Fig. 2A). We defined the average position of the feature centers in each chemical feature cluster as the center of common pharmacophore feature. The tolerances were set to the default values for corresponding features in Catalyst. The finally obtained common features are shown in Fig. 2A, which includes one hydrogen-bond acceptor (HA1), two hydrogen-bond donors (HD1 and HD2) and three hydrophobic features (H1, H2 and H3). Since the two features, HD1 and H1, approach closely (the distance between their centers is less than 1 Å), we thus constructed two five-feature pharmacophore hypotheses, Hypo1 and Hypo2 (Fig. 2B and C), with the other four features combined with either HD1 or H1, which is for the convenience of virtual screening.

2.2. Evaluations of the performances of Hypo1 and Hypo2 in virtual screening

In order to evaluate the performances of Hypo1 and Hypo2 in virtual screening, we built a test set, called M-ZINC. M-ZINC contains 110 known CK1 inhibitors (see Supplementary Table S1) and 3300 decoys [30] (the selection method for the decoys is given in the Supplementary data) from the ZINC chemical database [31]. The performance of virtual screening, including the yield (percentage of predicted compounds in known inhibitors), hit rate (percentage of known inhibitors in predicted compounds), and enrichment factor (ratio of hit rate to the percentage of known inhibitors in M-ZINC database), were evaluated.

The screening results are given in Table 1. From Table 1, we can see that the number of the predicted positives (Fitvalue ≥ 3.0) is 661, and that of the hits is 42 with a yield of 38.18% (42 out of the 110 inhibitors) for the use of Hypo1. The hit rate and enrichment
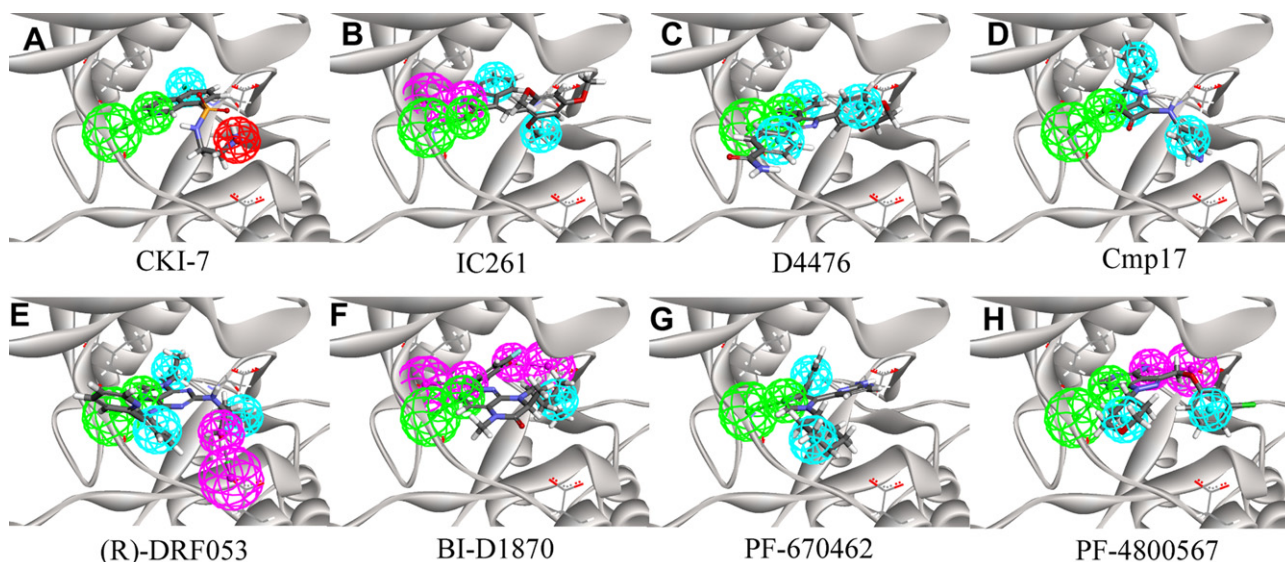

Fig. 1. The docking poses and pharmacophore models of eight known CK1 inhibitors in the crystal structure of CK1 (PDB code: 2CSN). (A)–(H) the green sphere represents hydrogen bond acceptor; puniceous represents the hydrogen bond donor; and light blue represents the hydrophobic feature. (For interpretation of the references to colour in this figure legend, the reader is referred to the web version of this article.)
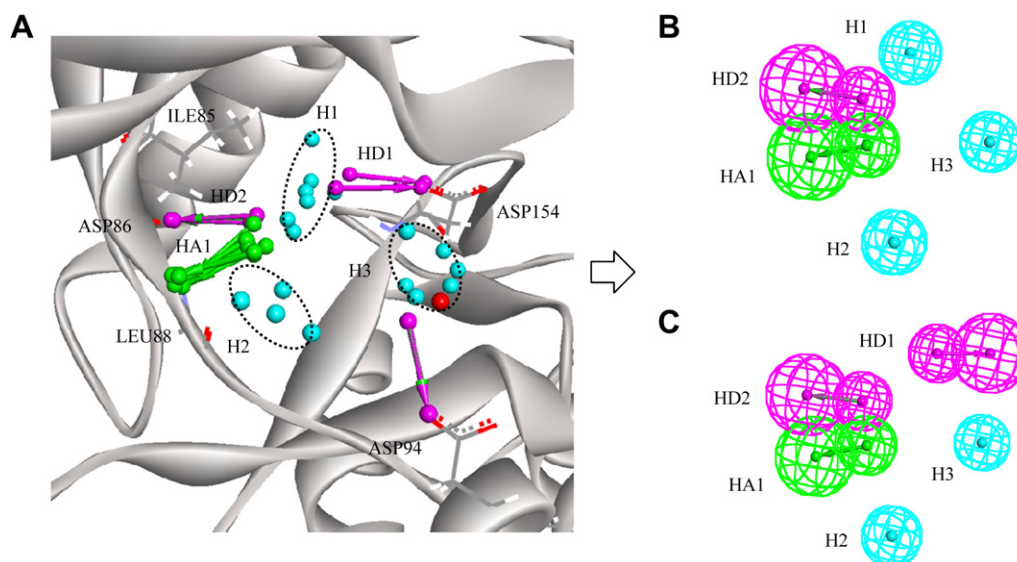
Fig. 2. Generation of common-feature pharmacophore models of CK1. (A) The superposition plot of the eight pharmacophore models. Hydrophobic features in dashed cycles represent the clustered hydrophobic features; (B) The pharmacophore model Hypo1; (C) The pharmacophore model Hypo2.

factor are 6.35% and 1.97, respectively. For Hypo2, the number of the predicted positives is 101, including 27 hits and 74 decoys; the yield is 24.55% (27 out of 110 inhibitors). The hit rate and enrichment factor for Hypo2 are 26.73% and 8.29, respectively. Here one may think that combined use of Hypo1 and Hypo2 may have a better performance compared with individual use of Hypo1 and Hypo2. We thus examined the effect of their combination. The yield, hit rate and enrichment factor are 41.82, 6.50 and 2.01, respectively. It is obvious that, though the yield increased a little, the hit rate and enrichment factor for the combined use of Hypo1 and Hypo2 drastically decreased compared with that for Hypo2. Considering that the hit rate and enrichment factor are the most concerned of in VS, Hypo2 was then chosen as the reference pharmacophore model in the subsequent VS for retrieving novel CK1 inhibitors.

2.3. Virtual screening and hit-to-lead optimization based on Hypo2

The optimal common feature pharmacophore model Hypo2 was used to screen several chemical databases including the commercial SPECS as well as an in-house chemical database to retrieve potential CK1 inhibitors with novel scaffolds. The number of maximum omitted features was set to 1. 50 compounds were finally selected from the top-ranking compounds sorted by Fitvalue (see Supplementary Table S2). Among them, the compound N6-(4-chlorophenyl)- 1*H*-pyrazolo[3,4-d]pyrimidine-3,6-diamine (**1**, Fig. 3A) attracted our attention due to that it possesses a novel scaffold and has the smallest molecular weight.

Fig. 3A depicts the mapping of **1** with Hypo2. From Fig. 3A, we can see that except one hydrophobic feature, the other four features are mapped very well. This mapping provides some important information, which could be used to guide the structural optimization of compound **1** (Fig. 3B). Firstly, a hydrophobic group could be added through a 'linker' to chlorobenzene to match the hydrophobic feature. Secondly, according to the orientations of H3 and H2, the "linker" added should be at the meta position (3-position) other than the para position (4-position) of phenyl. Thirdly, since the distance between the center of H2 and the center of H3 is about 8.5 Å, the 'linker' chain should be in the range of 4—5 bonds' length. Fourthly, there may exist a hydrogen bonding interaction between the 'linker' and the ASP94 (Fig. 1E). Fifthly, it would be better that the position of H3 hydrophobic feature is occupied by some aromatic rings, which is common in the known inhibitors. Based on these analyses, we designed 15 compounds, which are given in the Supplementary Figure S1. In the present work, we just chose three
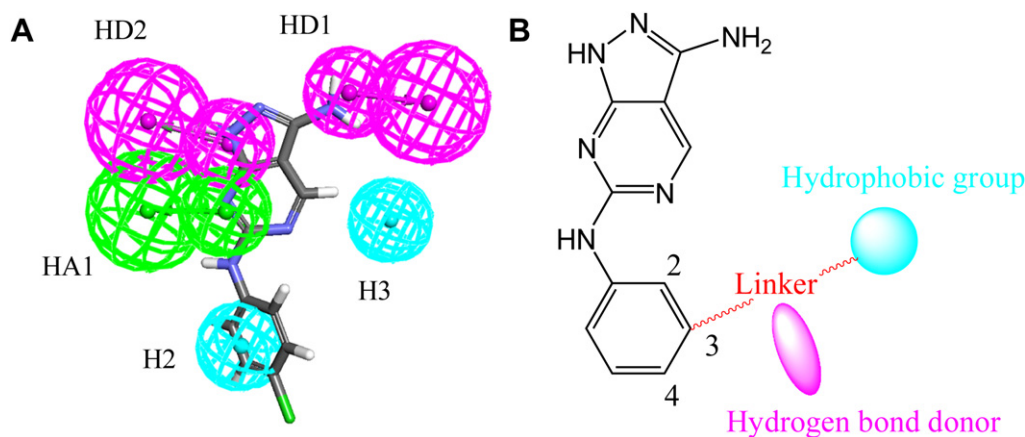

Fig. 3. Hit-to-lead optimization of compound **1** guided by Hypo2. (A) The mapping of the selected compound **1** from screening results to Hypo2; (B) The schematic of hit-to-lead optimization.
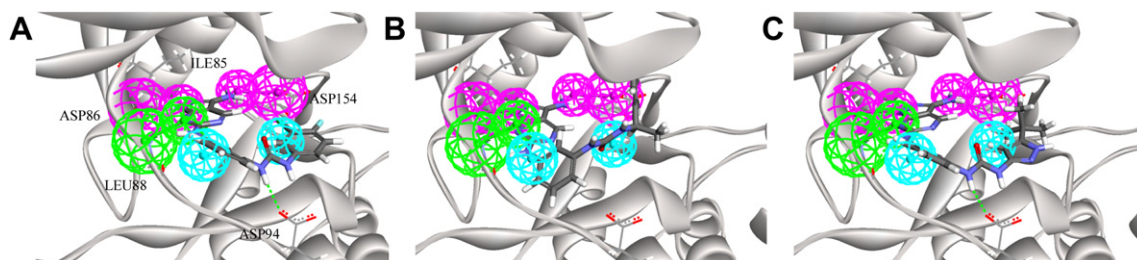
Fig. 4. The docking poses together with Hypo2 in the crystal structure of CK1 of (A) Compound **2**, (B) Compound **3** and (C) Compound **4**. The green dashed line represents hydrogen bond interaction. This interaction was predicted by using Discovery Studio 3.1 (Accelrys, Inc., USA). (For interpretation of the references to colour in this figure legend, the reader is referred to the web version of this article.)

representative compounds to synthesize since the main purpose here is to test the correctness of the pharmacophore model and our postulation. Synthesis of other compounds as well as further structural optimization will be carried out in succeeding studies, which results will be reported in the near future.

By the way, currently there are many rational design strategies for structural optimization to improve the potency of kinase inhibitors. For example, Liu and Gray [32] and Okram [33] have suggested a design strategy for the generation of type-II kinase inhibitors based on strategic placement of specific aryl amide or urea substituents onto a type-I inhibitor; type-II kinase inhibitors are generally thought to outperform corresponding type-I inhibitors in terms of the potency as well as the selectivity. The structural optimization strategy adopted here, which was based on and guided by the established pharmacophore model, could be another good option for the structural optimization of, not only kinase inhibitors, but also other hit compounds.

2.4. Chemistry

We then synthesized the selected three compounds, namely 1-(3-(3-amino-1*H*-pyrazolo[3,4-d]pyrimidin-6-ylamino)phenyl)-3-(3-chloro-4-fluorophenyl)urea (**2**), (R)-1-(3-(3-amino-1*H*-pyrazolo[3,4-d]pyrimidin-6-ylamino)phenyl)-3- (1-phenylethyl)urea (**3**), and 1-(3-(3-amino-1*H*-pyrazolo[3,4-d]pyrimidin-6-ylamino) phenyl)-3-(3-tert-butyl-1*H*-pyrazol-5-yl)urea (**4**). For comparison, we also synthesized two additional compounds, 1-(4-(3-amino-1*H*-pyrazolo[3,4-d]pyrimidin -6-ylamino)phenyl)-3-(3-chloro-4-fluorophenyl)urea (**5**), and (R)-1-(4-(3-amino-1*H*- pyrazolo[3,4-d]pyrimidin-6-ylamino)phenyl)-3-(1-phenylethyl)urea (**6**), in which the hydrophobic group is attached to the 4-position of phenyl.

A general scheme for the synthesis of compounds **2**−**6** is shown in Scheme 1. Reactions of commercially available 2-methyl-2-thiopseudourea sulfate (2:1) (**7**) with (E)-ethyl-2-cyano-3-ethoxyacrylate produced compound **8**, which was then reacted

CKI-7
IC$_{50}$=10uM

IC261
IC$_{50}$=1uM

D4476
IC$_{50}$=300nM

Cmp 17
IC$_{50}$=250nM

(R)-DRF053
IC$_{50}$=14nM

BI-D1870
IC$_{50}$=450nM

PF-670462
IC$_{50}$=80nM(CK1delta)
IC$_{50}$=130nM(CK1epsilon)

PF-4800567
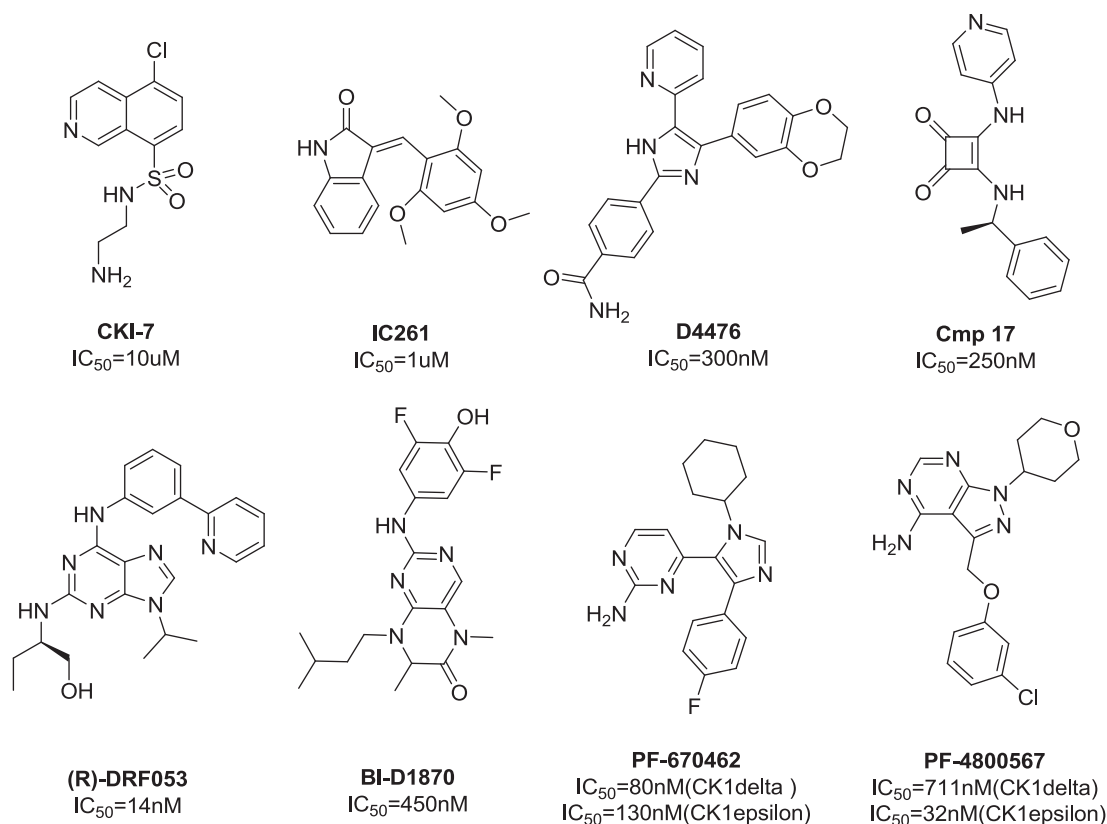IC$_{50}$=711nM(CK1delta)
IC$_{50}$=32nM(CK1epsilon)

Chart 1. Structures and activities of CK1 inhibitors in the training set.

Table 1
Comparison of the performances of Hypo1, Hypo2 as well as the combination of Hypo1 and Hypo2 in virtual screening against an independent test set, M-ZINC (110 CK1 inhibitors + 3300 decoys).

Model	Predicted positive	Number of hits	Yield (%)	Hit rate (%)	Enrichment factor
Hypo1	661	42	38.18	6.35	1.97
Hypo2	101	27	24.55	26.73	8.29
Hypo1+Hypo2	708	46	41.82	6.50	2.01

with phosphorus oxychloride to give compound **9**. Subsequently compound **9** was under cyclization reaction by using hydrazine hydrate to produce compound **10**, followed by addition of diluted hydrochloric acid to give compound **11**. Then, compound **11** was reacted with phosphorus oxychloride in the solvents of DMF and DMA to give the compound **12**. On the other side, the 3-nitroaniline or 4-nitroaniline (**13**) was reacted with isocyanates bearing different R_1 substituents to give the compound **14**, which was then reduced by using iron powder to provide compound **15**. Finally, the target compounds **2**–**6** were obtained from the reactions of compound **12** and **15** with different R1 substituents. More detailed description regarding reaction conditions and materials are given in Scheme 1 and Experimental section.

2.5. In vitro CK1 kinase inhibitory assay

Five synthesized compounds (listed in Table 2) were submitted to test their inhibitory potency against CK1. The IC_{50} values of these compounds against CK1 are given in Table 2. From Table 2, we can see that compound **2**, **3**, and **4**, in which the hydrophobic groups are linked to the 3-position of phenyl, have inhibition activity against CK1 with IC_{50} values being 78 nM, 2470 nM, and 142 nM,

respectively. Compound **5** and **6**, in which the hydrophobic groups are attached on the 4-position of phenyl, have no activity ($IC_{50} > 10$ μM). Fig. 4 depicts the interaction modes of **2**, **3** and **4** in the binding site of CK1, which shows that they all match very well in shape with the active pocket of CK1. Compound **2** has the best mapping with the hydrophobic feature (H3) compared with compound **3** and **4**. Compound **5** and **6** were also docked into the active site of CK1, which showed that there were some collisions occurred between **5**/**6** and residues of CK1, in addition to that H3 can not be mapped. These results are consistent with our analyses given above.

We further examined the selectivity of the most active compound. 12 common kinases, including ALK, Axl, mTOR, Plk1, Met, EGFR, CDK1, FGFR2, GSK3α, Flt3, PDGFRα, and KDR, were chosen. The inhibition activity was expressed as the percentage of the residual kinase activity with the concentration of the compound fixed at 10 μM. Table 3 presents the inhibition activity of compound **2** against CK1 and 12 selected kinases. From Table 3, we can see that compound **2** can completely inhibit the CK1 kinase activity (the inhibition rate = 100%) at the concentration of 10 μM. And it has also an inhibition rate greater than 90% against several other kinases including Met, EGFR, Flt3, and KDR, although it has a very low activity or almost no activity against the remaining seven kinases. All of these results indicate that compound **2** is not a good selective CK1 inhibitor. The optimization of the selectivity for this compound is still underway, for which results will be reported in the near future.
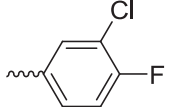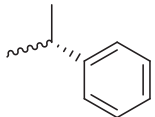
3. Conclusion
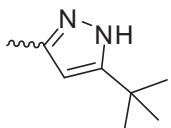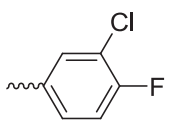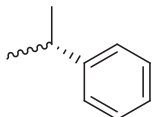
In this investigation, pharmacophore models of CK1 inhibitors were developed using a pharmacophore modeling protocol
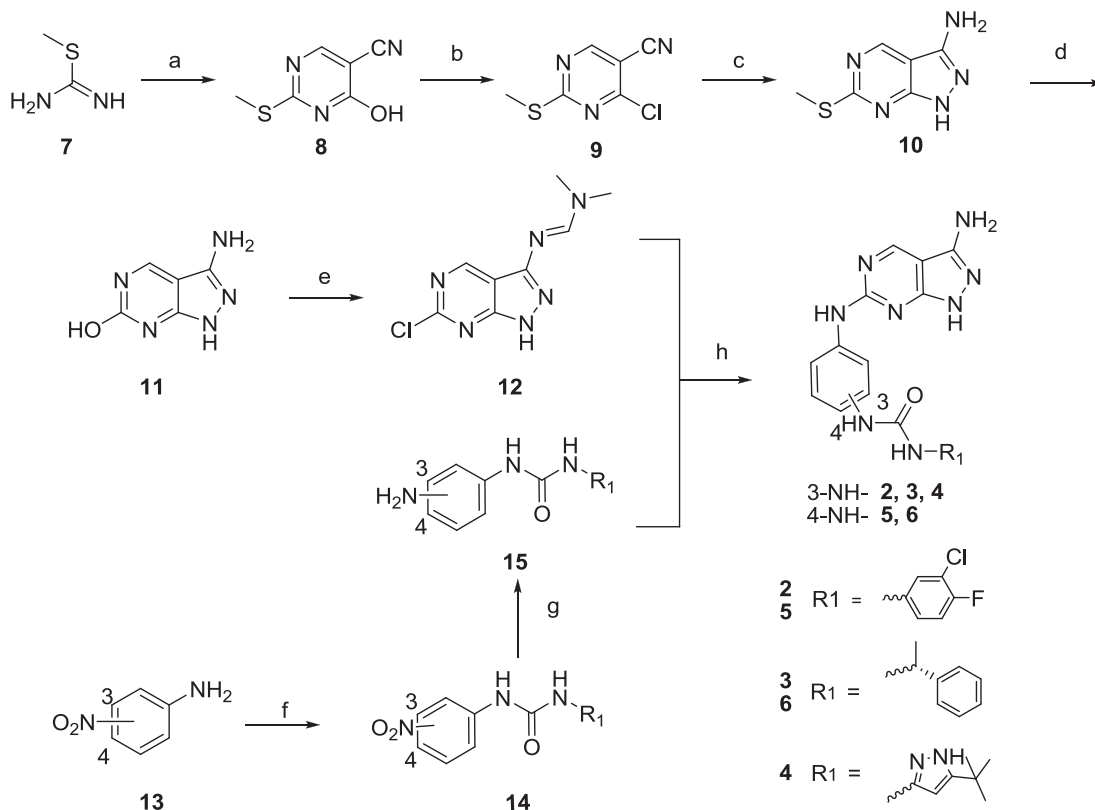
Scheme 1. Reagents and conditions: (a) (E)-ethyl-2-cyano-3-ethoxyacrylate, K_2CO_3, EtOH, H_2O, reflux, 12 h; (b) PhMe, Phosphorus oxychloride, reflux, 6 h; (c) (i) Hydrazine hydrate, n-Butanol, rt, 30 min; (ii) n-Butanol, reflux, 5 h; (d) EtOH, HCl, 80 °C, overnight; (e) Phosphorus oxychloride, DMF, DMA, 100 °C, 2 h; (f) (i) Triphosgene, Et_3N, THF, rt; (ii) R1–NH_2,THF, 45 °C, 2 h; (g) Fe, NH_4Cl, EtOH, H_2O, 1 h; (h) HCl, n-Butanol, 110 °C, 5 h.

Table 2
The kinase inhibition activity against CK1 of the designed compounds **2**–**6**.

Compound	Position	R_1	IC_{50} (nM)
2	3	Cl / F phenyl	78
3	3	phenyl (methyl)	2470
4	3	N–NH / t-butyl pyrazole	142
5	4	Cl / F phenyl	>10,000
6	4	phenyl (methyl)	>10,000

proposed by us. The optimal pharmacophore hypothesis, Hypo2, was adopted to retrieve potential CK1 inhibitors from the commercial chemical database SPECS and an in-house chemical database. Compound N6-(4-chlorophenyl)-1H-pyrazolo[3,4-d]

Table 3
The kinase inhibition activity of compound **2**.

Kinase	Inhibition (%) @10 μM
CK1	100
ALK	26
Axl	46
mTOR	0
Plk1	0
Met	99
EGFR	92
CDK1	42
FGFR2	35
GSK3α	34
Flt3	90
PDGFRα	82
KDR	96

pyrimidine-3,6-diamine was chosen from the top-ranking hits for further structural optimization since it is the smallest one and possesses a novel scaffold. A simple structural optimization, which was carried out under the guide of Hypo2, led to three active compounds with the highest one having an IC_{50} value of 78 nM against CK1. Collectively, this investigation reports the discovery of a lead compound targeting CK1 through a pharmacophore-based virtual screening and subsequent pharmacophore model guided structural optimization. This strategy used here could potentially be applied to the hit and lead discovery for other targets.

4. Experimental section

4.1. Docking calculations

All the docking calculations were performed using GOLD (version 5.0), which is one of the best docking programs [34]. The X-ray crystal structure of CK1 (PDB code 2CSN) [22] complexed with ligand CKI-7 was used as the reference receptor structure in the docking calculations. The preprocess of the protein structure was carried out by using Discovery Studio 3.1 (Accelrys, Inc., USA) software package, which includes removing all the water molecules, adding hydrogen and assigning the CHARMm forcefield. Then the binding site was defined as a sphere containing the residues that stay within 10 Å around the ligand in this crystal structure. Here we adopted the flexible docking strategy with the side chains of Val153, Leu138, Ser91, Asn136, Asp154 and Lys41 being set to flexible. The parameters used in the docking processes are given as follows: the 'Number of dockings' was set to 20 without constraints and early termination; the 'Detect Cavity' was turn on; 'Flip Ring Corners' was used to explore the rings conformations; the 'Flip Amide Bonds' was turn on; the planar of R-NRIR2 was flipped all and the protonated carboxylic acids were fixed; the genetic algorithm (GA) parameter was set as 'GOLD Default'.

4.2. Receptor–ligand pharmacophore generation

The 'Receptor–ligand pharmacophore generation' module of DS 3.1 program package was used to generate pharmacophore models. The parameters used are given as follows: the number features were delimited in the range of 3–6, and the 'Maximum pharmacophore' was set to 10; the option of 'Keep Water Molecules' and 'Add Shape Constraint' were both set to false; the maximum distances of charge, hydrogen bond and hypophobic group were set to 5.6, 3.2 and 5.5, respectively, and the minimum inter-feature distance was set to 2.0; the 'Check Pharmacophore' was turn on; and the others keep as default.

4.3. Chemistry

All the reagents were purchased from market and were used without further purification unless otherwise indicated. Analytical thin layer chromatography (TLC) was performed using aluminum sheet silica gel Merck 60F254, and the spots being developed with UV light. All the final compounds were purified to >95% purity, as determined by high-performance liquid chromatography (HPLC). [1] HNMR and ^{13}C NMR spectra were recorded on a Bruker AV-400 (400 MHz) spectrometer at 400 MHz and 100 MHz, respectively. Chemical shifts (δ) are quoted in parts per million (ppm) relative to tetramethylsilane (TMS) as an internal standard. Multiplicities are given as s (singlet), d (doublet), dd (double–doublet), q (quadruplet), t (triplet), and m (multiplet). Low-resolution and High-resolution mass spectral (MS) data were determined on an Agilent 1100 Series LCMS with UV detection at 254 nm and a low resonance electrospray mode (ESI).

4.3.1. 4-Hydroxy-2-(methylthio)pyrimidine-5-carbonitrile (8)

To a solution of 2-Methyl-2-thiopseudourea sulfate (19 g, 100 mmol) and (E)-ethyl 2-cyano-3-ethoxyacrylate (17 g, 100 mmol) in ethanol (380 ml), the K_2CO_3 solution (276 g, 200 mmol in 100 mL water) was added at room temperature. The reaction mixture was stirred at 85 °C overnight. The solvents were distilled on a rota-evaporator. The crude mixture was dissolved in water (100 ml) and adjusted the pH = 7–8 by using 6 N HCl. During the acidification, a buff solid was formed and collected by filtration. The filter cake was washed with a small amount of water and dried in a vacuum oven to give the product 8 (10.8 g). Yield: 65%; Purity: 92%; LC-MS m/z: 168.0 $[M + H]^+$.

4.3.2. 4-Chloro-2-(methylthio)pyrimidine-5-carbonitrile (9)

To a cooled solution of 4-hydroxy-2-(methylthio)pyrimidine-5-carbonitrile (8) (10.8 g, 65 mmol) in toluene (150 ml), phosphorus oxychloride (23.8 ml, 260 mmol) was slowly added. The reaction mixture was stirred at 110 °C for 6 h. After evaporation of the organic solvent, the residue was cooled to room temperature and added a lot of ice water. At this time, a brown solid was formed and collected by filtration. The crude product was dried in a vacuum oven to give 4-chloro-2-(methylthio)pyrimidine -5-carbonitrile 9(6.8 g). This product was taken up for the next step without any purification. Yield: 58%; Purity: 90%; LC-MS m/z: 186.0 $[M + H]^+$.

4.3.3. 6-(methylthio)-1H-pyrazolo[3,4-d]pyrimidin-3-amine (10)

A mixture of 4-chloro-2-(methylthio)pyrimidine-5-carbonitrile (9) (6.8 g, 36.5 mmol) and hydrazine hydrate (3.6 ml,73 mmol) in n-Butanol (120 ml) was stirred at room temperature for 0.5 h. Then, the solution was concentrated under reduced pressure. The residue was dissolved in n-Butanol (150 ml) and heated to reflux for 5 h, and the solution was concentrated again. The residue was washed with a small amount of water to give the product 6-(methylthio)-1H-pyrazolo[3,4-d]pyrimidin-3-amine (10) (6.05 g). Yield: 92%; Purity: 92%; LC-MS m/z:182.0 $[M + H]^+$. ^{1}H NMR (400 MHz, DMSO-d_6): δ12.28 (s, 1H), 8.88 (s, 1H), 5.97 (s, 2H), 2.51 (s, 3H)ppm.

4.3.4. 3-Amino-1H-pyrazolo[3,4-d]pyrimidin-6-ol (11)

A solution of 6-(methylthio)-1H-pyrazolo[3,4-d]pyrimidin-3-amine (10) (6.05 g, 33.2 mmol) in ethanol (45 ml) was added 6 N HCl (45 ml). The mixture was heated at 85 °C overnight and then cooled to room temperature, during which time a lot of yellow precipitate was formed. The resulting solid was collected by filtration to give the product 11 (4.04 g). Yield: 81%; Purity: 95%; LC-MS m/z:152.1 $[M + H]^+$. ^{1}H NMR (400 MHz, DMSO-d_6): δ12.62 (d, J = 6.8 Hz, 2H), 9.29 (s, 1H), 8.66 (s, 2H)ppm.

4.3.5. N′-(6-chloro-1H-pyrazolo[3,4-d]pyrimidin-3-yl)-N,N-dimethylformimidamide (12)

Phosphorus oxychloride (25 ml) was added to a mixture of 3-amino-1H-pyrazolo[3,4-d]pyrimidin-6-ol (11) (4.04 g, 26.7 mmol), DMF (3 ml) and DMA (2 ml). The resulting mixture was heated at 100 °C for 2 h. After cooling to room temperature, the redundant phosphorus oxychloride was removed. The residue was poured into ice-water and adjusted the pH to 7–8. Then the mixture was extracted several times with CH_2Cl_2. The final combined organic extracts were dried (Na_2SO_4) and concentrated under reduced pressure. The residue was then crystallized from ethyl acetate and petroleum ether to give the product 12 (3.25 g). Yield: 54%; Purity: 90%; LC-MS m/z: 225.1 $[M + H]^+$. ^{1}H NMR (400 MHz, DMSO-d_6): δ13.25 (s, 1H), 9.10 (s, 1H), 8.34 (s, 1H), 3.12 (s, 3H), 3.02 (s, 3H)ppm.

4.3.6. General procedure for synthesis of compounds 15

The nitroaniline (13) (1.38 g, 10 mmol) dissolved in THF (80 ml) was dropped slowly to a stirred solution of triphosgene (2.98 g,

10 mmol) in THF (10 mL) by using the constant pressure dropping funnel. NEt_3 (3 mL, 21 mmol) was then added slowly to the reaction mixture after the nitroaniline (13) was added completely. After evaporation of the organic solvent, THF (80 ml) and another amine (10 mmol) were added directly to the residue. The reaction mixture was stirred at 45°Cfor 2 h. The solvents were distilled on a rota-evaporator and the crude mixture was washed with water and acetone to give the product 14 (yield: 48%–71%).

The compound 14 (5 mmol) was taken in EtOH (30 mL), and iron powder (1.4 g, 25 mmol) was added at 50°C-55 °C followed by NH_4Cl solution (133 mg, 2.5 mmol in 15 mL water). The reaction mixture was refluxed for 1 h. Most of the iron powder was filtered while hot, the filtrate was concentrated under reduced pressure. The residue was dissolved in water (10 ml) basified with $NaHCO_3$ solution (pH 7–8) and extracted several times with ethyl acetate, the combined organic extracts were dried (Na_2SO_4), and concentrated under reduced pressure to furnish 9 (yield about 90%). This material was taken up for the next step without any purification.

4.3.7. 1-(3-(3-Amino-1H-pyrazolo[3,4-d]pyrimidin-6-ylamino) phenyl)-3-(3-chloro-4-fluorophenyl)urea (2)

6 N HCl (0.8 ml) was added to the mixture of 1-(3-aminophenyl)-3-(3-chloro-4-fluorophenyl)urea (15) (1.2 g, 4.4 mmol) in n-Butanol (20 ml). The reaction mixture was stirred at room temperature for 20 min. Then, a solution of (E)-N′-(6-chloro-1H-pyrazolo[3,4-d]pyrimidin-3-yl)-N,N-dimethylformimidamide (12) (1.0 g, 4.4 mmol) in n-Butanol (50 ml) was added into the former mixture and heated to 100 °C for 3.5 h. The solvent was distilled on a rota-evaporator. The crude mixture was added 100 ml water and the aqueous layer was extracted with ethyl acetate (2 × 120 ml). Then the combined organic layers were dried (Na_2SO_4) and concentrated. The residue was finally recrystallized from ethanol, ethyl acetate and petroleum ether to give the product 2 (1.52 g). Yield: 83%; Purity: 97%; LC-MS m/z: 413.1 $[M + H]^+$.^{1}H NMR (400 MHz, DMSO-d_6): δ11.77 (s, 1H), 9.56 (s, 1H), 8.88 (s, 1H), 8.80 (s, 1H), 8.72 (s, 1H), 7.82 (d, J = 3.2 Hz, 1H), 7.65 (s, 1H), 7.56 (s, 1H), 7.34–7.18 (m, 4H), 5.75 (s, 2H)ppm. ^{13}C NMR (100 MHz, DMSO-d_6): δ 158.3, 155.3, 152.5, 152.4, 148.6, 141.1, 139.4, 137.1, 128.6, 119.3, 118.4, 118.3, 116.9, 116.7, 113.3, 112.0, 109.4, 100.3 ppm.

4.3.8. 1-(4-(3-Amino-1H-pyrazolo[3,4-d]pyrimidin-6-ylamino) phenyl)-3-(3-chloro-4-fluorophenyl)urea (5)

The title compound was synthesized from 1-(4-aminophenyl)-3-(3-chloro-4- fluorophenyl)urea (15) (1.2 g, 4.4 mmol) and (E)-N′-(6-chloro-1H-pyrazolo[3,4-d] pyrimidin-3-yl)-N,N-dimethylformimidamide (12) (1.0 g, 4.4 mmol) using a procedure similar to that of 2. Yield: 81%; Purity: 98%; LC-MS m/z: 413.1 $[M + H]^+$. ^{1}H NMR (400 MHz, DMSO-d_6): δ11.76 (s, 1H), 9.58 (s, 1H), 8.80 (s, 1H), 8.52 (s, 1H), 8.30 (s, 1H),7.82 (s, 1H), 7.60 (d, J = 3.2 Hz, 2H), 7.34 (d, J = 4.4 Hz, 2H), 7.06 (d, J = 3.2 Hz, 2H), 5.72 (s, 2H)ppm. ^{13}C NMR (100 MHz, DMSO-d6): δ 158.2, 155.2, 152.7, 151.0, 148.6, 141.1, 137.2, 135.5, 133.1, 119.9, 119.5, 118.9, 118.3, 116.9, 116.7, 100.2 ppm.

4.3.9. (R)-1-(3-(3-amino-1H-pyrazolo[3,4-d]pyrimidin-6-ylamino) phenyl)-3-(1-phenyl ethyl) urea (3)

The title compound was synthesized from (R)-1-(3-aminophenyl)-3-(1-phenylethyl) urea (15) (1.1 g, 4.4 mmol) and (E)-N′-(6-chloro-1H-pyrazolo[3,4-d]pyrimidin-3-yl) -N,N-dimethylformimidamide (12) (1.0 g, 4.4 mmol) using a procedure similar to that of 2. Yield: 79%; Purity: 97%; LC-MS m/z: 389.2 $[M + H]^+$. ^{1}H NMR (400 MHz, DMSO-d_6): δ11.74 (s, 1H), 9.47 (s, 1H), 8.78 (s, 1H), 8.33 (s, 1H), 7.48 (d, J = 6.0 Hz, 2H), 7.34 (d, J = 6.0 Hz, 4H), 7.26–7.23 (m, 1H), 7.16–7.08 (m, 2H), 6.61 (d,J = 8.0 Hz 1H), 5.73 (s, 2H), 4.83–4.80 (m, 1H), 1.38 (d, J = 7.2 Hz, 3H)ppm. ^{13}C NMR (100 MHz, DMSO-d_6): δ 158.4, 155.3, 154.3, 152.4, 148.6, 145.2, 140.9,

140.4, 128.5, 128.3, 126.6, 125.8, 112.5, 111.2, 108.6, 100.4, 48.5, 23.1 ppm.

4.3.10. (R)-1-(4-(3-amino-1H-pyrazolo[3,4-d]pyrimidin-6-ylamino)phenyl)-3-(1-phenylethyl) urea (6)

The title compound was synthesized from (R)-1-(4-aminophenyl)-3-(1-phenylethyl) urea (15) (1.1 g, 4.4 mmol) and (E)-N'-(6-chloro-1H-pyrazolo[3,4-d]pyrimidin-3-yl) -N,N-dimethylformimidamide (12) (1.0 g, 4.4 mmol) using a procedure similar to that of 2. Yield: 79%; Purity: 98%; LC-MS *m/z*: 389.2 [M + H]⁺. ¹H NMR (400 MHz, DMSO-d_6): δ11.68 (s, 1H), 9.38 (s, 1H), 8.74 (s, 1H), 8.23 (s, 1H), 7.63 (d, *J* = 8.8 Hz, 2H), 7.34 (d, *J* = 4.0 Hz, 4H), 7.27—7.23 (m, 3H), 6.54 (d, *J* = 8.0 Hz, 1H), 5.69 (s, 2H), 4.83—4.80 (m, 1H), 1.37 (d, *J* = 6.8 Hz, 3H)ppm.

4.3.11. 1-(3-(3-Amino-1H-pyrazolo[3,4-d]pyrimidin-6-ylamino) phenyl)-3-(5-tert-butyl-1H-pyrazol-3-yl) urea (4)

The title compound was synthesized from 1-(3-aminophenyl)-3-(5-tert-butyl -1H-pyrazol-3-yl)urea (15) (1.2 g, 4.4 mmol) and (E)-N'-(6-chloro-1H-pyrazolo[3,4-d] pyrimidin-3-yl)-N,N-dimethylformimidamide (12) (1.0 g, 4.4 mmol) using a procedure similar to that of 2. Yield: 79%, Purity: 98%; LC-MS *m/z*: 407.2 [M + H]⁺. ¹H NMR (400 MHz, DMSO-d_6): δ11.98 (s, 1H), 11.80 (s, 1H), 9.65 (s, 1H),9.15 (b, 1H), 9.00 (s, 1H), 8.89 (s, 1H), 7.65 (s, 1H), 7.52 (d, *J* = 7.2 Hz, 1H), 7.21—7.15 (m, 2H), 5.80 (s, 2H),1.41 (s, 9H)ppm. ¹³C NMR (100 MHz, DMSO-d_6): δ 158.3, 155.3, 152.9, 152.4, 152.0, 148.6, 147.4, 140.9, 139.6, 128.6, 113.3, 111.9, 109.4, 100.4, 90.6, 30.6, 29.9 ppm.

4.4. In vitro kinase inhibitory assay

All the kinase inhibitory assays were carried out through the KinaseProfiler service provided by Millipore [35]. CK1 was incubated with 200 μM specific substrate KRRRALS(p)VASLPGL, 10 mM MgAcetate and [γ-³³P-ATP] (specific activity approx. 500 cpm/pmol, concentration as required). The buffer composition includes 20 mM MOPS, 1 mM EDTA, 0.01% Brij-35, 5% Glycerol, 0.1% β-mercaptoethanol, and 1 mg/ml BSA. The reaction was initiated by the addition of the MgATP mix. After incubation for 40 min at room temperature, the reaction was stopped by the addition of 3% phosphoric acid solution. 10 μL of the reaction was then spotted onto a P30 filtermat and washed three times for 5 min in 75 mM phosphoric and once in methanol prior to drying and scintillation counting. IC$_{50}$ values of compounds were determined from dose—response curves obtained from the assays at 10 different concentrations of each compound. All the assays were repeated twice and the mean values of activity were calculated.

Appendix A. Supplementary material

Supplementary data associated with this article can be found in the online version, at http://dx.doi.org/10.1016/j.ejmech.2012.08.007. These data include MOL files and InChiKeys of the most important compounds described in this article.

References

[1] U. Knippschild, A. Gocht, S. Wolff, N. Huber, J. Lohler, M. Stoter, The casein kinase 1 family: participation in multiple cellular processes in eukaryotes, Cell. Signal. 17 (2005) 675—689.

[2] O. Marin, V.H. Bustos, L. Cesaro, F. Meggio, M.A. Pagano, M. Antonelli, C.C. Allende, L.A. Pinna, J.E. Allende, A noncanonical sequence phosphorylated by casein kinase 1 in beta-catenin may play a role in casein kinase 1 targeting of important signaling proteins, Proc. Natl. Acad. Sci. U. S. A. 100 (2003) 10193—10200.

[3] J.K. Cheong, D.M. Virshup, Casein kinase 1: complexity in the family, Int. J. Biochem. Cell. Biol. 43 (2011) 465—469.

[4] D.P. Hanger, H.L. Byers, S. Wray, K.Y. Leung, M.J. Saxton, A. Seereeram, C.H. Reynolds, M.A. Ward, B.H. Anderton, Novel phosphorylation sites in tau from Alzheimer brain support a role for casein kinase 1 in disease pathogenesis, J. Biol. Chem. 282 (2007) 23645—23654.

[5] D.I. Perez, C. Gil, A. Martinez, Protein kinases CK1 and CK2 as new targets for neurodegenerative diseases, Med. Res. Rev. 31 (2011) 924—954.

[6] N.P. Shanware, J.A. Hutchinson, S.H. Kim, L. Zhan, M.J. Bowler, R.S. Tibbetts, Casein kinase 1-dependent phosphorylation of familial advanced sleep phase syndrome-associated residues controls PERIOD 2 stability, J. Biol. Chem. 286 (2011) 12766—12774.

[7] S. Luz, P. Kongsuphol, A.I. Mendes, F. Romeiras, M. Sousa, R. Schreiber, P. Matos, P. Jordan, A. Mehta, M.D. Amaral, K. Kunzelmann, C.M. Farinha, Contribution of casein kinase 2 and spleen tyrosine kinase to CFTR trafficking and protein kinase A-induced activity, Mol. Cell. Biol. 31 (2011) 4392—4404.

[8] U. Knippschild, S. Wolff, G. Giamas, C. Brockschmidt, M. Wittau, P.U. Wurl, T. Eismann, M. Stoter, The role of the casein kinase 1 (CK1) family in different signaling pathways linked to cancer development, Onkologie 28 (2005) 508—514.

[9] P. Gribbon, A. Sewing, Fluorescence readouts in HTS: no gain without pain? Drug Discov. Today 8 (2003) 1035—1043.

[10] D.B. Kitchen, H. Decornez, J.R. Furr, J. Bajorath, Docking and scoring in virtual screening for drug discovery: methods and applications, Nat. Rev. Drug Discov. 3 (2004) 935—949.

[11] P.D. Lyne, Structure-based virtual screening: an overview, Drug Discov. Today 7 (2002) 1047—1055.

[12] G. Klebe, Virtual ligand screening: strategies, perspectives and limitations, Drug Discov. Today 11 (2006) 580—594.

[13] H. Eckert, J. Bajorath, Molecular similarity analysis in virtual screening: foundations, limitations and novel approaches, Drug Discov. Today 12 (2007) 225—233.

[14] P. Gedeck, R.A. Lewis, Exploiting QSAR models in lead optimization, Curr. Opin. Drug Discov. Dev. 11 (2008) 569—575.

[15] N. Brown, R.A. Lewis, Exploiting QSAR methods in lead optimization, Curr. Opin. Drug Discov. Dev. 9 (2006) 419—424.

[16] P.R. Murumkar, V.P. Zambre, M.R. Yadav, Development of predictive pharmacophore model for in silico screening, and 3D QSAR CoMFA and CoMSIA studies for lead optimization, for designing of potent tumor necrosis factor alpha converting enzyme inhibitors, J. Comput. Aided. Mol. Des. 24 (2010) 143—156.

[17] S.Y. Yang, Pharmacophore modeling and applications in drug discovery: challenges and recent advances, Drug Discov. Today 15 (2010) 444—450.

[18] G.B. Li, L.L. Yang, S. Feng, J.P. Zhou, Q. Huang, H.Z. Xie, L.L. Li, S.Y. Yang, Discovery of novel mGluR1 antagonists: a multistep virtual screening approach based on an SVM model and a pharmacophore hypothesis significantly increases the hit rate and enrichment factor, Bioorg. Med. Chem. Lett. 21 (2011) 1736—1740.

[19] S. Thangapandian, S. John, S. Sakkiah, K.W. Lee, Potential virtual lead identification in the discovery of renin inhibitors: application of ligand and structure-based pharmacophore modeling approaches, Eur. J. Med. Chem. 46 (2011) 2469—2476.

[20] P. Purushottamachar, J.B. Patel, L.K. Gediya, O.O. Clement, V.C. Njar, First chemical feature-based pharmacophore modeling of potent retinoidal retinoic acid metabolism blocking agents (RAMBAs): identification of novel RAMBA scaffolds, Eur. J. Med. Chem. 47 (2012) 412—423.

[21] J. Zou, H.Z. Xie, S.Y. Yang, J.J. Chen, J.X. Ren, Y.Q. Wei, Towards more accurate pharmacophore modeling: multicomplex-based comprehensive pharmacophore map and most-frequent-feature pharmacophore model of CDK2, J. Mol. Graph. Model. 27 (2008) 430—438.

[22] R.M. Xu, G. Carmel, J. Kuret, X. Cheng, Structural basis for selectivity of the isoquinoline sulfonamide family of protein kinase inhibitors, Proc. Natl. Acad. Sci. U. S. A. 93 (1996) 6308—6313.

[23] N. Mashhoon, A.J. DeMaggio, V. Tereshko, S.C. Bergmeier, M. Egli, M.F. Hoekstra, J. Kuret, Crystal structure of a conformation-selective casein kinase-1 inhibitor, J. Biol. Chem. 275 (2000) 20052—20060.

[24] F. Lovering, S. Kirincich, W. Wang, K. Combs, L. Resnick, J.E. Sabalski, J. Butera, J. Liu, K. Parris, J.B. Telliez, Identification and SAR of squarate inhibitors of mitogen activated protein kinase-activated protein kinase 2 (MK-2), Bioorg. Med. Chem. 17 (2009) 3342—3351.

[25] G. Rena, J. Bain, M. Elliott, P. Cohen, D4476, a cell-permeant inhibitor of CK1, suppresses the site-specific phosphorylation and nuclear exclusion of FOXO1a, EMBO Rep. 5 (2004) 60—65.

[26] N. Oumata, K. Bettayeb, Y. Ferandin, L. Demange, A. Lopez-Giral, M.L. Goddard, V. Myrianthopoulos, E. Mikros, M. Flajolet, P. Greengard, L. Meijer, H. Galons,

Roscovitine-derived, dual-specificity inhibitors of cyclin-dependent kinases and casein kinases 1, J. Med. Chem. 51 (2008) 5229–5242.

[27] G.P. Sapkota, L. Cummings, F.S. Newell, C. Armstrong, J. Bain, M. Frodin, M. Grauert, M. Hoffmann, G. Schnapp, M. Steegmaier, P. Cohen, D.R. Alessi, BI-D1870 is a specific inhibitor of the p90 RSK (ribosomal S6 kinase) isoforms in vitro and in vivo, Biochem. J. 401 (2007) 29–38.

[28] K.M. Walton, K. Fisher, D. Rubitski, M. Marconi, Q.J. Meng, M. Sladek, J. Adams, M. Bass, R. Chandrasekaran, T. Butler, M. Griffor, F. Rajamohan, M. Serpa, Y. Chen, M. Claffey, M. Hastings, A. Loudon, E. Maywood, J. Ohren, A. Doran, T.T. Wager, Selective inhibition of casein kinase 1 epsilon minimally alters circadian clock period, J. Pharmacol. Exp. Ther. 330 (2009) 430–439.

[29] Z. Zhou, A.K. Felts, R.A. Friesner, R.M. Levy, Comparative performance of several flexible docking programs and scoring functions: enrichment studies for a diverse set of pharmaceutically relevant targets, J. Chem. Inf. Model. 47 (2007) 1599–1608.

[30] N. Huang, B.K. Shoichet, J.J. Irwin, Benchmarking sets for molecular docking, J. Med. Chem. 49 (2006) 6789–6801.

[31] J.J. Irwin, B.K. Shoichet, ZINC–a free database of commercially available compounds for virtual screening, J. Chem. Inf. Model. 45 (2005) 177–182.

[32] Y. Liu, N.S. Gray, Rational design of inhibitors that bind to inactive kinase conformations, Nat. Chem. Biol. 2 (2006) 358–364.

[33] B. Okram, A. Nagle, F.J. Adrian, C. Lee, P. Ren, X. Wang, T. Sim, Y. Xie, G. Xia, G. Spraggon, M. Warmuth, Y. Liu, N.S. Gray, A general strategy for creating "inactive-conformation" abl inhibitors, Chem. Biol. 13 (2006) 779–786.

[34] G. Jones, P. Willett, R.C. Glen, A.R. Leach, R. Taylor, Development and validation of a genetic algorithm for flexible docking, J. Mol. Biol. 267 (1997) 727–748.

[35] Millipore Inc. KinaseProfiler Servce http://www.millipore.com/life_sciences/flx4/ld_kinases.